Theory and simulation of epitaxial rotation: Light particles adsorbed on graphite

Eduard Vives* and P. A. Lindgård
Risø National Laboratory, DK-4000 Roskilde, Denmark
(Received 22 June 1992; revised manuscript received 26 October 1992)

We present a theory and Monte Carlo simulations of adsorbed particles on a corrugated substrate. We have focused on the case of rare gases and light molecules, H_2 and D_2, adsorbed on graphite. The competition between the particle-particle and particle-substrate interactions gives rise to frustration phenomena. From our model predictions for the epitaxial rotation angle of the adsorbed phases are determined. Our results extend and unify previously known descriptions. We have studied as a function of temperature and coverage the phase diagrams, especially the intermediate phases appearing between the commensurate and incommensurate phase for the adsorbed systems. From our simulations and our theory, we are able to understand the γ phase of D_2 as an ordered phase stabilized by disorder. It can be described as a $2q$-modulated structure. In agreement with the experiments, we have also found a modulated 4×4 structure. Energy, structure-factor intensities, peak positions, and epitaxial rotation angles as a function of temperature and coverage have been determined from the simulations. Good agreement with theory and experimental data is found.

I. INTRODUCTION

In the last two decades, considerable effort has been devoted to understanding the properties of matter in two dimensions. Several theories have been developed[1,2] which predict a dramatic difference between phase transition in two-dimensional (2D) and three-dimensional (3D) systems. One of the major problems in testing existing theories is that very few experimental systems are really 2D. Apart from measurements on liquid-crystal films,[3] most of the systems studied are surface layers on solid or liquid substrates.[2] Thus, it is important to study the role of the perturbing substrate on the 2D physical properties. A related problem, intensively studied in recent years, is frustration. Frustration is usually associated with an incompatibility between the topology of the system and the interactions. For instance, antiferromagnetic ordering cannot classically be uniquely established on a fcc lattice. In this case quantum or thermal fluctuations can select a stable ground state among the large number of classically degenerated ones.[4] Another example, still not fully understood, is the nucleation of a compact (fcc or hexagonal) phase in a bcc phase, which occurs at the martensitic phase transition.[5] Such phase transitions occur in a large number of pure metals, metallic alloys, and ceramics. In this case, the frustration arises from the incompatible symmetry of the two phases.

In this paper we demonstrate that perturbed 2D systems also exhibit frustration, though different from that described above. Examples of such systems are adsorbed atoms or molecules on crystalline surfaces,[6] and the layers in the intercalated compounds.[7] The particles of the 2D layer interact through different kinds of particle-particle potentials: Metallic ions with a screened Coulomb interaction, rare gases with Van der Waals forces, etc. The particles interact with the substrate (or with adjacent layers, in the case of intercalated compounds) with a potential that we can consider to have two parts: (i) an attractive binding force between the adsorbed particles and the substrate, which depends upon the distance of the particles from the substrate, and (ii) a corrugation potential having the translational symmetry of the substrate, which depends upon the horizontal position of the particles. At high temperatures the 2D liquid phase consequently shows modulations with the substrate symmetry and the corrugation potential can be measured via the structure factor.[8] At low temperatures, and for a range of coverages, the particle-particle interaction produces a structure incompatible with that which minimizes the corrugation potential energy. This gives rise to frustration. We distinguish two cases: (i) the optimal adsorbate structure has a different symmetry than the one imposed by the substrate, for example, rare gases which prefer a close-packed structure adsorbed on the square lattice of MgO(100) (Ref. 9); (ii) the two structures have the same symmetry but different lattice parameters. We will focus on the latter case, paying special attention to the systems with hexagonal symmetry, such as the light molecules (H_2 and D_2), and the rare gases adsorbed on the graphite basal plane. Our theory can also be formulated for case (i) and is expected to yield similar conclusions to those discussed below.

Detailed experimental measurements of 2D-systems' phase diagrams exist as a function of the temperature and coverage (i.e., density) of adsorbed particles. Accurate phase transition lines have been measured by calorimetry.[10–13] Also the structure of different phases has been determined using diffraction techniques, including x-rays,[14] transmission high-energy electron diffraction (THEED),[15] low-energy electron diffraction (LEED),[16,17] and neutron diffraction.[18] At low temperatures, and as a function of increasing coverage, from zero to completion of the first monolayer, these phase diagrams exhibit at least the following sequence of phases: fluid, a coexistence region, a commensurate phase, and an incommensurate phase. The commensurate phase is, for the

cases in which we are interested, the $\sqrt{3}\times\sqrt{3}$ phase for which the preferred distance between the particles is $\sqrt{3}$ times the graphite lattice spacing.

The existence of frustration in the system manifests itself in two interesting phenomena: (i) the epitaxial rotation exhibited by the incommensurate structure,[19] and (ii) the appearance of intermediate phases between the commensurate and the fully incommensurate structures.[20] Our main objective is to develop a model and to perform Monte Carlo (MC) computer simulations in order to clarify these two points.

Epitaxial rotation is a general phenomenon resulting from the interactions between two incommensurate structures. It optimizes the particle-substrate interaction. Several theories,[19] based on the elastic properties of the adsorbate and substrate, have been developed to explain the epitaxial rotation angle as a function of the misfit between the two structures. These have successfully described the epitaxially rotated and nonrotated phases, and the transition between them for heavy rare gases adsorbed on graphite. However, a number of experimental results corresponding to the lighter atoms or molecules [D_2 (Ref. 18), Li/Rb (Ref. 21)] do not fit into the picture of the existing theories. We will try to provide an explanation for these cases.

The nature of the transition between the incommensurate and commensurate phases and the existence of disordered or complicated ordered phases in the intermediate region is still under discussion. On the basis of a study of all the possible commensurate structures (coincidence lattice theory[22]) and different 1D theories,[23,24] it has been proposed that a devil's staircase may appear.[25] In the case of light particles adsorbed on graphite, indications of several intermediate phases have been measured.[18,12,13,11,17] But their real-space structure is, in some cases, unknown. In general, they exhibit epitaxial rotation angles in disagreement with the existing theories.[19]

In the conventional description of adsorbed monolayers, the problem is simplified to a domain competition between the three equivalent registered A, B, and C domains. And the behavior is determined by the domain-wall energy. We have found that this picture breaks down in the high-density regime, since there such "registered domains" are exceedingly small (sometimes just one particle) and most of the system consists of "domain walls." These walls are, furthermore, strongly relaxed. This makes it also difficult to use the Moiré pattern argumentation. Generally, we shall by a domain mean a region of a single phase. Thus, for example, one domain of the 4×4 structure consists of many one-particle A, B, and C registered domains. Instead of domain, we will sometimes use the word "grain" in order to reduce the possibility of confusion.

We will concentrate primarily on the case of D_2 and H_2 on graphite, for which extensive experimental data exist. Calorimetric measurements[12,13] have revealed the existence of intermediate phases between the commensurate and the fully incommensurate phases. Some of these are not fully understood. The existence of and nature of a striped α phase is still under discussion,[18,17,26] and so is the nature of the γ phase. This phase exhibits a surprisingly large epitaxial rotation angle.[17,26] A further modulated ϵ phase within the γ phase, detected by the specific-heat measurements, has not been revealed by the scattering data.[12] The structure of these phases is unknown because it is difficult for the scattering experiments to access the region of large wave vectors and to obtain data which is not averaged radially (due to the lack of single-crystal measurements). ^{4}He on graphite[11] is another system which exhibits intermediate phases.

The paper is organized as follows. In Sec. II A we present a model describing a hexagonal adsorbate on a rigid hexagonal substrate. In Sec. II B we discuss the particle-particle interaction between the adsorbed particles in our model. In Secs. II C and II D we analyze the influence of the deformations and the finite size of the adsorbate on the epitaxial rotation angle. In Sec. III A we present the details of the MC simulations. The choice of parameters for the case of D_2 and H_2 on graphite is discussed in Sec. III B. In Sec. III C we present our MC results and compare with experimental results. Finally, Sec. IV summarizes and concludes.

II. THEORY

A. Model

Let us consider a system of N particles adsorbed on a hexagonal substrate with lattice parameter a. There are N_s lattice cells. The coverage is defined as $\rho=3N/N_s$. Since we are interested in the phase diagram for coverages less than a complete monolayer, we will only consider the projection of the particle positions on the substrate. The projected 2D Hamiltonian H is defined as

$$H=-k_BT\ln\left[\int dz_1\cdots dz_i\cdots dz_N e^{-H^{3d}/k_BT}\right], \quad (1)$$

where z_i represents the z component of the ith particle on the substrate and H^{3d} is the nonprojected Hamiltonian. Let $\mathbf{r}_i$ be the 2D vectors describing the projections of the particle positions on the substrate plane. We assume that the Hamiltonian for the projected variables can be split in a term (H_0) containing the particle-particle pair interactions and another term (H_1) containing the substrate-particle interaction

$$H=H_0+H_1=\sum_{ij}^{\text{pairs}}V(\mathbf{r}_{ij})+\sum_{i}^{N}U(\mathbf{r}_i), \quad (2)$$

where $\mathbf{r}_{ij}=\mathbf{r}_i-\mathbf{r}_j$. For H_2, D_2, and the rare gases, over the range of temperatures in which we are interested, it is a good approximation to assume that the particle-particle interaction is isotropic $V(\mathbf{r})=V(r)$. The particle-substrate potential interaction U can be Fourier expanded as

$$U(\mathbf{r})=\sum_{HK}U_{HK}e^{i\mathbf{Q}_{HK}\cdot\mathbf{r}}, \quad (3)$$

where $\mathbf{Q}_{HK}$ are the reciprocal-lattice vectors of the substrate. The U_{00} term represents the average adsorption energy per particle. It keeps the particles on the sub-

strate. If the coverage is constant, U_{00} does not influence the phase transitions between different, planar, ordered structures. For symmetry reasons, a number of terms are equal. For instance, $U_{10}=U_{01}=U_{1-1}=U_{-11}=U_{0-1}=U_{-10}$ correspond to the six equivalent reciprocal vectors of the substrate lattice: Q_{10}, Q_{01}, Q_{1-1}, Q_{-11}, Q_{0-1}, and Q_{-10}. We will call this set of reciprocal space positions the (1,0) star, Q^*_{10}. As a first approximation to the problem it is assumed that U_{10} is much bigger than the subsequent terms, like U_{11} belonging to Q^*_{11}. For the case of light molecules adsorbed on graphite, this is a good approximation. In the case of heavier atoms or molecules strongly chemisorbed on the substrate, like Rb on graphite, the higher-order terms have been measured. Even in that case, the values are fairly small $U_{11}\simeq 0.1U_{10}$.[27]

We define the structure factor of the system $S(\mathbf{q})$ as

$$S(\mathbf{q})=|\hat{\rho}(\mathbf{q})|^2 , \quad \hat{\rho}(\mathbf{q})=\sum_{j=1}^{N} e^{i\mathbf{q}\cdot\mathbf{r}_j} . \tag{4}$$

Using these definitions the Hamiltonian (2) can be Fourier transformed, yielding

$$\begin{aligned} H&=H_0+H_1 \\ &=\int [S(\mathbf{q})-N]\hat{V}(q)d\mathbf{q} \\ &\quad+\int \hat{\rho}(\mathbf{q})\sum_{HK} U_{HK}\delta(\mathbf{q}-\mathbf{Q}_{HK})d\mathbf{q} , \end{aligned} \tag{5}$$

where $\hat{V}(q)$ is the 2D Fourier transformation of $V(r)$, which will be further discussed in Sec. II B. In general it is an oscillating function which decays with increasing q (Fig. 1). Therefore, only the small wave-vector region of $S(\mathbf{q})$ will be important. Equation (5) shows that the present problem represents a particular case of frustration. Namely, a competition between the particle-particle interaction H_0, which is an integral continuously extending in all the reciprocal space, and the particle-substrate interaction, which is an integral of a set of δ functions at the discrete vectors $\mathbf{q}=\mathbf{Q}_{HK}$.

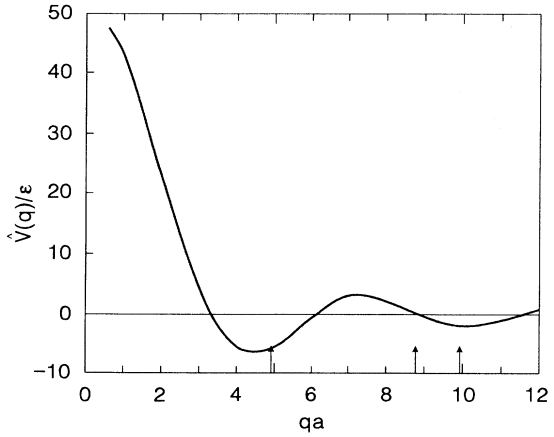

FIG. 1. Fourier transform $\hat{V}(q)$ of the particle-particle interaction used in our simulations. The arrows indicate the positions of the reciprocal vectors corresponding to the perfect hexagonal lattice with $q_{10}=4\pi/(\sqrt{3}r_0)$.

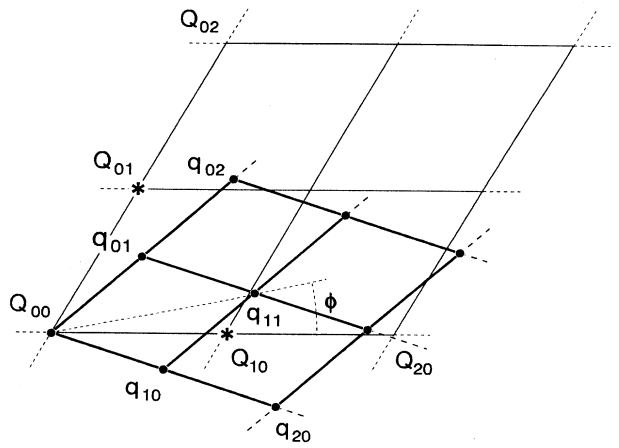

FIG. 2. The reciprocal lattices of the adsorbate and the substrate, and the definition of the epitaxial rotation angle ϕ.

In the thermodynamic limit ($N\to\infty$, $N_s\to\infty$, $N/N_s=\rho/3$), and at low temperatures, a perfect hexagonal structure for the adsorbate minimizes the particle-particle energy. For this $S(\mathbf{q})$ has a infinite number of equal intensity Bragg peaks at the reciprocal-lattice vectors $\mathbf{q}_{hk}$. If the structure is incommensurate $|\mathbf{q}_{hk}|\neq|\mathbf{Q}_{HK}|$, there will be no contribution from the particle-substrate energy. Therefore, the system will be (continuously) orientationally degenerate. The relevant experiments on adsorbed monolayers are close to the commensurate $\sqrt{3}\times\sqrt{3}$ structure (i.e., $|\mathbf{q}_{10}|\sim|\mathbf{Q}_{10}|/\sqrt{3}$). We will focus on this case. We define the epitaxial rotation angle ϕ as the angle between $\mathbf{q}_{11}$ and $\mathbf{Q}_{10}$. Hence $\phi=0$ for the commensurate $\sqrt{3}\times\sqrt{3}$ structure. Figure 2 schematically represents the first two reciprocal-space cells of the substrate, indicating the positions of a number of substrate ($\mathbf{Q}_{hk}$) and adsorbate ($\mathbf{q}_{hk}$) reciprocal vectors and the definition of ϕ.

Elastic deformations, defects, or finite-size effects will produce diffuse scattering extending $S(\mathbf{q})$ and $\hat{\rho}(\mathbf{q})$ in all reciprocal space, thus always giving a nonzero value of H_1. This value, regardless of its magnitude, breaks the infinite degeneracy of the ground state and selects an appropriate epitaxial rotation angle ϕ. The destruction of the perfect hexagonal adsorbate structure results from the competition described by Eq. (5). Energetically small contributions are responsible for the rotation of the whole system, making it difficult to develop theories for the epitaxial rotation in complete agreement with experimental results. In 2D there is additionally the interesting phenomenon that true long-range order does not exist.[28]

B. Particle-particle interaction, $V(r)$

In order to further proceed, the main characteristics of the projected interaction $V(r)$ between the adsorbed particles on the substrate must be analyzed. The systems of rare gases are, in 3D, well described by the 6–12 Lennard-Jones potential

$$V_{LJ}(r)=4\epsilon\{(\sigma/r)^{12}-(\sigma/r)^{6}\}\ , \tag{6}$$

where σ and ϵ are parameters. The potential shows an infinite repulsion as $r\to 0$, preventing an overlap of particles, and it has a minimum at $r_0=2^{1/6}\sigma$. For the molecular systems H_2 and D_2, a Lennard-Jones interaction has been useful describing the 3D phase diagram at low densities.[29] After the projection to 2D, we expect that the potential will still exhibit a minimum at an approximately similar distance (r_0) as in the 3D case. However, the infinite hard-core repulsion will be smoothed since the particles at small distances can escape to the third dimension by jumping to the second layer at only a finite cost of energy. This justifies the introduction of a cutoff at short distances $r<r_1$.

In our MC simulations, we have used the following modified 2D Lennard-Jones potential

$$V(r)=\begin{cases} V_0 & \text{if } r<r_1 \\ 4\epsilon\{(\sigma/r)^{12}-(\sigma/r)^{6}\} & \text{if } r_1<r<r_2 \\ 0 & \text{if } r>r_2 \end{cases} \tag{7}$$

with $r_1=2\sqrt{3}a/3$ and $r_2=5\sqrt{3}a/3$.[30] For the range of temperatures and coverages in our investigation, we have tested that the r_1 cutoff is irrelevant (i.e., no jump attempts have been accepted to the flat V_0 region; this ensures that no particles occupy the same substrate well). The effect of the long distance cutoff r_2 is mainly a shift in the energy, which has been discussed in a previous paper.[30]

The Fourier transform of $V(r)$ is in 2D

$$\begin{aligned}\hat{V}(q)&=\int_0^{\infty} rV(r)dr\int_0^{2\pi} e^{iqr\cos\theta}d\theta \\ &=\frac{2}{\pi}\int_0^{\infty} rV(r)J_0(qr)dr\ ,\end{aligned} \tag{8}$$

where $J_0(x)$ is the zero-order Bessel's function. For a potential $V(r)\sim 1/r^n$ to be integrable, it is required (i) that it diverges more slowly than or at the same rate as $1/r$, when $r\to 0$ and (ii) that it decreases more rapidly than $1/r^{1.5}$ when $r\to\infty$. For the projected potential, we have supposed that $V(r\to 0)\to V_0$, where V_0 is related to the energy required for the promotion of the particles to the second layer. This ensures convergence in case (i). Furthermore, at large distances the 6–12 potential satisfies condition (ii).

Potentials with a hard-core finite cutoff [$V(r)=V_0$ for $r<r_1$] will exhibit minima in $\hat{V}(q)$. However, if $V_0\to\infty$, the position of the first minimum will be at $q_{\min}=5.136/r_1$, independent of the behavior of the rest of the potential. For finite values of V_0 the position of $q_{\min}$ is determined by both the cutoff r_1 and the position of the minimum of $V(r)$ at r_0. An example is shown in Fig. 1, where the Fourier transform of the potential in Eq. (7) is displayed for typical parameters used in our simulations. We see that the first minimum of $\hat{V}(q)$ is displaced to smaller values of q than that corresponding to the minimum of $V(r)$ [$q_0=(4\pi/\sqrt{3})r_0^{-1}$]. The shift in the minimum of $\hat{V}(q)$ is due to both the existence of the cutoff r_1, and to the fact that the structure factor $S(\mathbf{q})$ minimizing the energy exhibits a set of δ functions, so the other minima of $\hat{V}(q)$ must be taken into account in the integral in Eq. (5). At high temperatures, the Bragg peaks of the structure are smeared out due to disorder, in particular for large values of q. The average energy is then determined principally by the first Bragg peak at ($|\mathbf{q}_{10}|$), and an energy minimum is obtained when the position shifts from q_0 to $q_{\min}$. This gives an explanation for the expansion of the lattice for increasing temperatures.

C. Deformations of the system

As shown in Sec. II A, for a perfect, incommensurate, hexagonal adsorbate, there is no contribution from the particle-substrate potential, so no preferred epitaxial rotation angle is selected. Let us now suppose that the adsorbate lattice is distorted. This may arise from temperature fluctuations, defects, local elastic relaxations,.... The positions of the particles are given by $\mathbf{r}_j=\mathbf{R}_j+\mathbf{u}_j$, where $\mathbf{R}_j$ corresponds to the positions of a perfect hexagonal structure and $\mathbf{u}_j$ to the displacements. For small distortions, $\hat{\rho}(\mathbf{q})$ [Eq. (4)], can be, classically, expanded to first order as

$$\hat{\rho}(\mathbf{q})=\hat{\rho}_0(\mathbf{q})+i\sum_{j=1}^{N}\mathbf{q}\cdot\mathbf{u}_j e^{i\mathbf{q}\cdot R_j}+\cdots\ . \tag{9}$$

We express the distortion field as a combination of waves

$$\mathbf{u}_j=\int d\mathbf{q}\ \mathbf{A}(\mathbf{q})e^{i\mathbf{q}\cdot\mathbf{R}_j}\ , \tag{10}$$

where the integral extends over the first Brillouin zone of the adsorbate reciprocal lattice $\{q_{hk}\}$ and $\mathbf{A}(\mathbf{q})$ is the complex vector amplitude exhibiting different symmetries, depending upon the physical mechanism that produces the distortions. In general, if the displacements field $\mathbf{u}(\mathbf{R}_k)\equiv\mathbf{u}_k$ is invariant under a rotation R^{θ}, $\mathbf{A}(\mathbf{q})$ is also invariant, i.e.,

$$\mathbf{u}(R^{\theta}\mathbf{R})=R^{\theta}\mathbf{u}(\mathbf{R})\Leftrightarrow\mathbf{A}(R^{\theta}\mathbf{q})=R^{\theta}\mathbf{A}(\mathbf{q})\ . \tag{11}$$

Note, that since $\mathbf{R}=\{\mathbf{R}_j\}$, only rotations R^{θ} that are symmetry operations of the perfect adsorbate lattice are allowed. Since the displacements $\mathbf{u}_j$ are real, we always have

$$\mathbf{A}(\mathbf{q})=[\,\mathbf{A}(-\mathbf{q})]^{*}\ . \tag{12}$$

We now calculate the contribution to the particle-substrate energy H_1 using Eqs. (9), (10), and (5),

$$\begin{aligned}H_1&=U_{10}\sum_{\mathbf{Q}\in\mathbf{Q}_{10}^{*}}\hat{\rho}(\mathbf{Q}) \\ &=iNU_{10}\sum_{\mathbf{Q}\in\mathbf{Q}_{10}^{*}}\mathbf{Q}\cdot\mathbf{A}(\mathbf{q}_{\underline{hk}}-\mathbf{Q})\ ,\end{aligned} \tag{13}$$

where $\mathbf{q}_{\underline{hk}}$ is the reciprocal vector of the perfect adsorbate which is closest to $\mathbf{Q}$ [in our case $\mathbf{q}_{\underline{hk}}=\mathbf{q}_{11}$, for $\mathbf{Q}=\mathbf{Q}_{10}$, and the corresponding symmetry related relationships for the other members of the (1,0)-star]. We denote by $\delta\mathbf{q}$ any element of the set of six vectors $\mathbf{q}_{\underline{hk}}-\mathbf{Q}$ with $\mathbf{Q}\in\mathbf{Q}_{10}^{*}$. Since H_1 is real, we have

$$\mathbf{A}(\delta\mathbf{q}) = -\mathbf{A}(-\delta\mathbf{q}) \tag{14}$$

which, according to Eq. (11), implies that the expansion of the density in Eq. (9) only makes physical sense if there is an inversion symmetry point in the displacement field $u(\mathbf{R}_j)$. Note in Eq. (13) that predominantly the components of the distortion amplitudes parallel to the substrate reciprocal lattice contribute to the energy. For symmetry reasons we expect this property to persist even for expansions to higher order in $\mathbf{u}_j$. The exact minimization of H_0+H_1, required for calculating the epitaxial rotation angle, is difficult, but symmetry considerations about the vector amplitude $\mathbf{A}(\delta\mathbf{q})$ lead to a determination of the preferred orientational angle. We distinguish two cases.

(a) If the distortions are governed by the elastic behavior of the adsorbate, the function $\mathbf{A}(\delta\mathbf{q})$ will be determined by the phonon frequencies $\omega(\mathbf{q})$. $|\mathbf{A}(\delta\mathbf{q})|$ will show a starlike shape with maximum values oriented according to the direction of the softest branch. Usually, it is the transverse branch with $\delta\mathbf{q}\|\mathbf{q}_{10}^*$.

(b) In the low-coverage regions, around defects (vacancies, for instance), the particles will relax toward the substrate wells according to the substrate potential force,

$$\mathbf{F}_j = -\nabla U(\mathbf{R}_j) \simeq -iU_{10} \sum_{\mathbf{Q}\in\mathbf{Q}_{10}^*} \mathbf{Q} e^{i\mathbf{Q}\cdot\mathbf{R}_j} . \tag{15}$$

Such a perturbation will produce nonisotropic deformations around the defects, oriented according to the substrate symmetry.[31] In this case, the maximum amplitude will occur for $\delta\mathbf{q}\|\mathbf{Q}_{10}^*$.

Figure 3 shows the different geometries of cases (a) and (b). For consistency, we also show two other cases, (c) and (d), corresponding to $\mathbf{A}(\delta\mathbf{q})$ having maximum intensity for $\delta\mathbf{q}\|\mathbf{q}_{11}^*$ and $\delta\mathbf{q}\|\mathbf{Q}_{11}^*$, respectively, although no simple physical explanation can be given for these cases at this stage. (Later we will analyze how these possibilities can appear from other mechanisms.)

Minimization of the particle-substrate energy in Eq. (5) for these four cases gives the following relations between the misfit $m=\sqrt{3}q_{10}/Q_{10}$, and the epitaxial rotation angle ϕ,

$$m = \frac{\tan\beta}{\cos\phi\tan\beta - \sin\phi} , \tag{16}$$

with the four possibilities $\beta=30°+\phi$, 60°, $60°+\phi$, and 30° for cases (a), (b), (c), and (d), respectively. The epitaxial angles determined by these four relations are shown in Fig. 4. It is interesting that these conditions were found by Grey and Bohr[32] by phenomenological considerations of Moiré patterns and by making use of a symmetry principle. Here we demonstrate that they naturally arise, assuming the model in Eq. (1). The tendency for the diffuse scattering coming from the distortions to be aligned with respect to the $\mathbf{Q}_{10}^*$ [case (b)] was already pointed out in connection with measurements of D_2 on graphite.[17]

The unrotated solution $\phi=0$ must also be considered. In fact, case (c) is always metastable relative to the unrotated solution, since, from elastic considerations, we expect that $|\mathbf{A}(\delta\mathbf{q})|$ decays monotonically with $|\delta\mathbf{q}|$ and the unrotated solution represents a smaller value of $|\delta\mathbf{q}|$. The solution (b), based on the defect mechanism, is also metastable relative to the unrotated solution if $|\mathbf{A}(\delta\mathbf{q})|$ decays monotonically. On the other hand, if the defects form any kind of superlattice, the monotonic decay cannot be assumed.

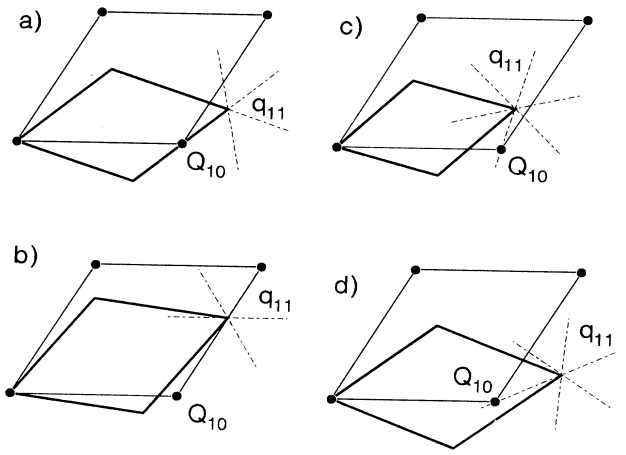

FIG. 3. Schematic representation of the four possible relations for the epitaxial rotation angle. The dashed-dotted lines represent the main symmetry directions of the diffuse scattering around the $\mathbf{q}_{11}$ Bragg point. Case (a) corresponds to the usual elasticity mechanism, (b) corresponds to the vacancy stabilization mechanism, and (c) and (d) are plotted for completion. In cases (b) and (d), the orientation of the dashed-dotted star does not change when rotating the adsorbate on the substrate, while in cases (a) and (c) it rotates with the adsorbate lattice.

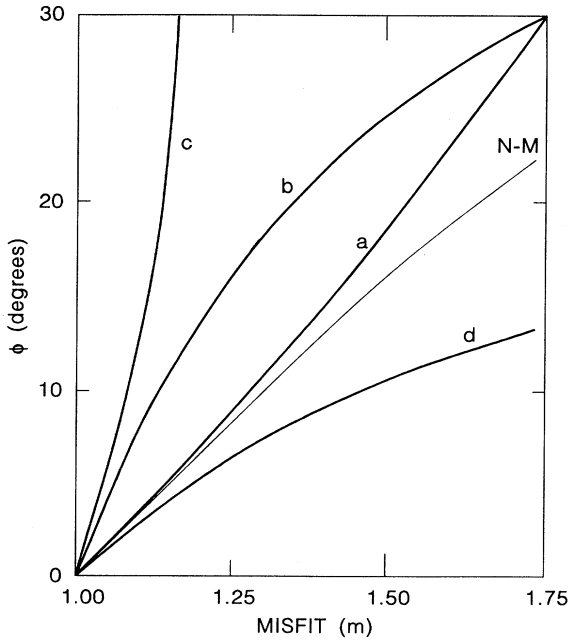

FIG. 4. Display of the (a), (b), (c), and (d) relations for the epitaxial rotation Eq. (16), together with the Novaco-McTague relation (Ref. 19) for a Lennard-Jones adsorbate.

The results of Eq. (16), as shown in Fig. 4, reproduce a number of experimental measurements of ϕ obtained by changing the adsorbate coverage and the temperature (thus the misfit) for different systems: the rotated incommensurate phase of Ar,[33] D_2, H_2, and HD (Ref. 17) on graphite, and Na on Rb,[21] is described by Eq. (16) for the case corresponding to stabilization by elastic deformations [case (a)] and Ne on graphite,[16] Li on Rb,[21] and the intermediate phase of D_2 on graphite[17] is described by the case corresponding to stabilization due to local deformations around defects [case (b)]. Some of this data was presented in support of the symmetry principle.[32] Phases with an epitaxial rotation angle stabilized by defects only appear in the case of light particles (D_2, Ne, Li) for which the preferred distance between the particles is sufficiently small compared to the $\sqrt{3}\times\sqrt{3}$ structure. As will be discussed in Sec. III B, the preferred distance between H_2 molecules is larger than that between the D_2 molecules due to the quantum zero-point motion. The change in parameters [in Eq. (5)] has the consequence that H_2 does not exhibit intermediate phases with the epitaxial rotation angle stabilized by defects, as it is the case for D_2.

The present theory for epitaxial rotation unifies some previously known descriptions. Case (a) is an approximation to the well-known Novaco-McTague-Villain-Shiba theory,[19] which has been successfully applied to Ar, Kr, and Xe atoms adsorbed on graphite. For these systems, the corrugation is smaller and the preferred distance closer to the $\sqrt{3}\times\sqrt{3}$ structure. However, it does not explain some of the phases that appear in phase diagrams of the lighter molecules. The theory explicitly derives the position of the maximum value of $\mathbf{A}(\delta\mathbf{q})$ for different systems having different values of the transverse (c_T) and longitudinal (c_L) elastic constants. The maximum depends on the parameter $\eta=(c_L/c_T)^2-1$. In Fig. 4 we plot the prediction of their theory for $\eta=2$, which corresponds to a Cauchy solid, as exemplified by the presently discussed Lennard-Jones system.

Case (b) suggests a hitherto neglected possibility for a defect-stabilized epitaxial rotation angle. In the next sections we will show that this provides an explanation for some intermediate phases appearing in the phase diagrams for D_2 and ^{4}He adsorbed on graphite. In fact, the relation (b) can be derived from a further development of the theory of Reiter and Moss[8] for corrugated modulated liquids. They show that the first ring in the liquid-structure factor $S(q)$ is modulated in a way that the $\mathbf{q}_{10}$ peak appears. If the misfit $m>1$, the position of the peak $\mathbf{q}_{10}$ arises from the overlap of the first ring with the one centered at $\mathbf{Q}_{10}$, fulfilling $|\mathbf{q}_{10}|=|\mathbf{q}_{10}-\mathbf{Q}_{10}|$. This condition is identical to the relation (b) $(\mathbf{q}_{11}-\mathbf{Q}_{10})\|\mathbf{Q}_{01}$. Since a liquid ring also appears centered on the $\mathbf{Q}_{01}$ position, the stabilized structure factor shows both $\mathbf{q}_{10}$ and $\mathbf{q}'_{10}$ peaks corresponding to the equivalent $+\phi$ and $-\phi$ rotation angles. We characterize this as a $2q$-modulated structure in contrast to the structure stabilized from relation (a) in which the two peaks $\mathbf{q}_{10}$ and $\mathbf{q}'_{10}$ appear from the coexistence of different single-q domains, i.e., domains of structures characterized each by only one principal wave vector.

Our results are derived for structures close to the commensurate $\sqrt{3}\times\sqrt{3}$ structure for which $\mathbf{Q}_{10}=\mathbf{q}_{11}$. They can be generalized to other cases of misfit. The stabilization of other perfect commensurate structures, for which there is an exact match between $\mathbf{Q}_{10}$ and other $\mathbf{q}_{hk}$ has been carefully studied by the so-called coincidence lattice theory.[22] This theory yields a set of discrete possible values on the (m,ϕ) diagram for which $\mathbf{q}_{hk}=\mathbf{Q}_{HK}$. These values fall on lines similar to those shown in Fig. 4. Most of these structures, for the range of misfits considered here, can only be stabilized by assuming that the substrate potential has large contributions from other terms than U_{10}, usually U_{HK} for very large values of H and K. However, in our simulations we have found agreement with a "semicoincidence" lattice theory, in which it is enough that the projection of any Bragg peak $\mathbf{q}_{hk}$ in a high symmetry direction equals the projection of $\mathbf{Q}_{10}$. We could also call this a case of an uniaxially incommensurate phase. The stabilization of such a phase can be justified from finite domain size effects, as we will show in the next section.

D. Finite-size effects

The selection of the epitaxial rotation angle is sensitive to any mechanism that yields diffuse scattering around the main Bragg peaks. We must therefore also consider the effect of the finite size and shape of the adsorbate regions—either islands or grains. The island case has previously been studied numerically by Grey and Bohr[32] for selected hexagonal shapes. The theory underlying this is discussed below, on the basis of Eq. (5).

Let $S_f(\mathbf{r})$ be a shape function that takes the value 1 in the region covered by a uniform adsorbate with perfect structure, and 0 outside this region. $\hat{\rho}(\mathbf{q})$ for a finite hexagonal adsorbate can be written as

$$\hat{\rho}(\mathbf{q})=\int \hat{S}_f(\mathbf{q}')\hat{\rho}_\infty(\mathbf{q}-\mathbf{q}')d\mathbf{q}' , \tag{17}$$

where $\hat{\rho}_\infty(\mathbf{q})$ corresponds to the infinite adsorbate and $\hat{S}_f(\mathbf{q})$ is the Fourier transform of $S_f(\mathbf{r})$. Substituting Eq. (17) into the Hamiltonian Eq. (5), we obtain the following expression for the particle-substrate interaction:

$$H_1=\int \hat{\rho}_\infty(\mathbf{q})\sum_{HK} U_{HK}\hat{S}_f(\mathbf{q}-\mathbf{Q}_{HK})d\mathbf{q} . \tag{18}$$

Comparison with Eq. (5) shows that the finite size of the crystal destroys the δ-function-like peaks of the particle-substrate interaction. Of the infinite number of adsorbate Bragg peaks $\mathbf{q}_{hk}$, the one which is closest to $\mathbf{Q}_{10}$ is $\mathbf{q}_{11}$ for the case in which we are interested, so we can approximate

$$H_1\simeq 6U_{10}\hat{S}_f(\mathbf{q}_{11}-\mathbf{Q}_{10}) . \tag{19}$$

In this equation there is an implicit minimization with respect to small displacements of the center of adsorbate region inside a substrate unit cell. Such translations produce a phase change of the $\hat{S}_f$ function. It can be shown that there exists a phase for which H_1 takes the optimum

value equal to that of Eq. (19).

In general, the energy per area $H_1/\hat{S}_f(0)$ is an oscillatory function changing very quickly with the size R and orientation of the adsorbate region. It decays like $1/(|\delta\mathbf{q}|R)^2$. Thus, we conclude that the epitaxial rotation angle is completely dominated by finite-size effects if $R \lesssim 1/|\delta\mathbf{q}|$. We start by considering the effect of a finite circular domain. The function $\hat{S}_f(\delta\mathbf{q})$, is in this case, independent of the orientation of $\mathbf{q}$. From Eq. (19) we obtain

$$H_1 = 12U_{10}(\pi R^2)\frac{J_1(|\delta\mathbf{q}|R)}{|\delta\mathbf{q}|R} , \tag{20}$$

where R is the radius of the region and J_1 is the first-order Bessel function. A geometrical analysis yields the following relationship between $|\delta\mathbf{q}|$, the misfit m, and the epitaxial rotation angle ϕ:

$$|\delta\mathbf{q}| = |\mathbf{q}_{11} - \mathbf{Q}_{10}| = \frac{4\pi}{a\sqrt{3}}\sqrt{m^2 - 2m\cos\phi + 1} . \tag{21}$$

Substituting this into Eq. (19), and minimizing with respect to ϕ for different values of m and R, allows the determination of a preferred orientation due to finite-size effects only. Figure 5 shows an example for the case $R = 10a$. We see a set of intervals where the systems prefers to be unrotated, and discrete jumps to different rotated branches. For increasing radius, the density of jumps and their height increase, covering all the (m,ϕ) space as $R \to \infty$. This indicates that no epitaxial rotation angle is preferred for the infinite, perfect, fully incommensurate structure. These results may explain some recent experiments for Xe adsorbed on graphite[14] in which first-order-like transitions (with hysteresis) have been seen between nonrotated and slightly rotated branches with a curvature similar to that observed in Fig. 5.

When the regions are not circular, more complicated phenomena may appear. We distinguish two different cases for the shape dependence of H_1 and the epitaxial rotation angle ϕ: (i) The shape of the finite region is defined by the shape of the substrate, i.e., when the adsorbate rotates the shape does not; (ii) the shape of the finite region is determined only by the adsorbate, so it rotates with ϕ. We call R^ϕ the rotation operator associated with the epitaxial rotation angle. The two dependences (i) and (ii) can be written as

$$\text{(i)}\ H_1 = 6U_{10}\hat{S}_f(R^\phi\mathbf{q}_{11} - \mathbf{Q}_{10}) , \tag{22}$$

$$\text{(ii)}\ H_1 = 6U_{10}\hat{S}_f[R^{-\phi}(R^\phi\mathbf{q}_{11} - \mathbf{Q}_{10})] . \tag{23}$$

For irregular shapes it is difficult to proceed further, but for hexagonal substrates on hexagonal adsorbates we expect that the islands or grains will also exhibit hexagonal symmetry. (This is, in fact, the basis of the "symmetry principle" of Bohr and Grey[32]). Assuming that the function $\hat{S}_f(\delta\mathbf{q})$ has maximum values along high-symmetry directions (0° or 30°), we can from Eqs. (22) and (23) easily derive the four conditions described in Fig. 4 and Eq. (16). Thus we obtain the same relations from two different physical mechanisms. This makes it difficult to distinguish from experimental results which mechanism is the most important. If the regions are striped, the function $\hat{S}_f(\mathbf{q})$ will be elongated in the direction perpendicular to the stripe. In this case we can justify the "semicoincidence" lattice theory that has been mentioned in the previous section.

Most experimental data fall on lines (a) and (b) of Fig. 4. Cases (c) and (d) can only be justified when finite-size effects are important or when the $\mathbf{Q}_{11}^*$ terms in the expansion of Eq. (3) are the dominant ones.

We note that the present theory can be reformulated for the case of a rigid adsorbate on a deformable substrate, yielding the same relations for the epitaxial rotation angle, but with the opposite physical explanations. This last possibility is less frequently realized in experiments. A recent calculation of the interfacial energy for the case of fcc(111)/bcc(110) epitaxy[34] leads to similar conclusions with respect to the role played by the finite size of the adsorbate. Further experiments and analysis concerning correlation between the epitaxial rotation angle, the facets of the adsorbate islands or grains, and the existence of steps on the substrate are needed in order to clarify the importance of finite-size effects in the determination of the epitaxial rotation angle. The presence of steps and minute amounts of impurities may, in fact, completely dominate the epitaxial rotation. This was demonstrated experimentally for Kr/Pt(111).[35] A motivation for the present Monte Carlo simulation study is to be able to study realistic size samples and yet to avoid the influence of such effects.

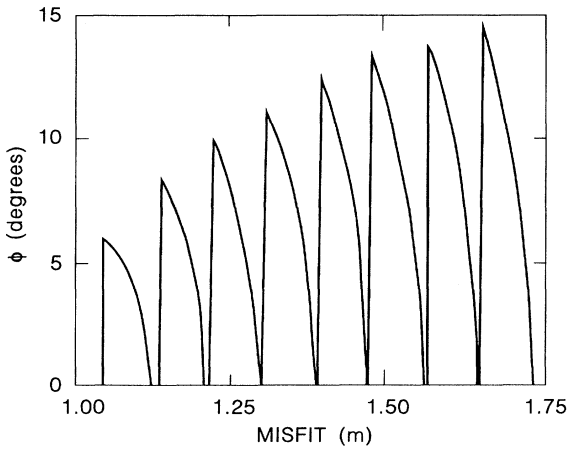

FIG. 5. Epitaxial rotation angle determined by finite-size effects for a circular region of size $R = 10a$ as a function of the misfit m.

III. MONTE CARLO SIMULATION

A. Details

We have used a conventional Metropolis algorithm to simulate the model[30] for the case of D_2 and H_2 on graphite. A number of particles N ranging between 1000 and 4000 have been placed on a substrate with $90\times90=8100$ cells and periodic boundary conditions. During each

Monte Carlo step (MCS), N attempts are made to displace a particle on the surface. Each proposed displacement is a random 2D vector uniformly distributed in a circle of radius R_{max}. For $R_{max}=0.2a$, at least 10% of the attempts are accepted for low temperatures and high coverage. The large size of the system allows us to measure the structure factor $S(\mathbf{q})$ with a resolution of 90×90 points in each reciprocal space lattice cell. Averages over the six equivalent directions of the hexagonal lattice are made to improve the statistics of our results. The initial configuration for the simulations is a disordered state equilibrated during 5×10^4 MCS at high temperature ($k_BT/\epsilon=6.0$). For the case $N=2700(\rho=1)$ simulations started from an ordered $\sqrt{3}\times\sqrt{3}$ structure have also been done. Averages of the interesting quantities have typically been taken over 50–100 configurations, separated by $10^3-5\times10^3$ MCS after an equilibration time of $2\times10^4-5\times10^4$ MCS. In addition, averaging over 3–5 independent runs have been made. Stabilization of the low-temperature phases was achieved after three or four successive stepwise quenches. These consisted of simulating over a long time ($\sim10^4$ MCS) at the desired final temperature T, then reheating to higher temperature ($\sim2T$), and slowly cooling down to temperature T. The cycle was then repeated with slower cooling rates. This method helps enormously in the growth of the ordered domains and in resolving the small satellites in $S(\mathbf{q})$. Equilibration problems are probably associated with the existence of first-order phase transitions. We have applied the same treatment to all the independent runs for different coverages, so that even in case that equilibrium is not completely reached, we can still compare our results. The phase diagram discussed in Sec. III C was determined using temperature scans starting from the low-temperature, equilibrated phases, and heating by steps of $k_B\Delta T/\epsilon\sim0.02$. Most of the simulations have been carried out using an Apollo 10000 work station. The duration of a typical run for a given temperature is 8–10 CPU hours, and the total amount of time expended is about 2×10^3 CPU hours.

B. Parameters for D_2 and H_2

The model [Eq. (2)] contains four parameters $(a,\sigma,U_{10},\epsilon)$. Defining ϵ and a as units of energy and length, respectively, we reduce the number of free parameters to two dimensionless parameters: $\sigma^*=\sigma/a$ and $U^*=-U_{10}/\epsilon$. The lattice parameter for graphite is $a=2.456$ Å. We also similarly define a dimensionless temperature $T^*=k_BT/\epsilon$. Estimates for the parameters (σ^*,U^*) can be obtained from the literature. Since first-principles calculations are complicated for 2D quantum systems, most of the existing data comes from the corresponding 3D systems. The behavior of the 3D solid rare gases is well described by an isotropic Lennard-Jones interaction,[36] and estimates of σ and ϵ are known in this case. Although a Lennard-Jones potential does not fully reproduce the interaction between D_2 and H_2 molecules, a fit to the 3D gas-phase isotherms gives $\epsilon/k_B=36.2$ K, $\sigma=2.95$ Å for D_2 and $\epsilon/k_B=36.7$ K, $\sigma=2.96$ Å for H_2. A discussion of these two parameters is given by Silvera.[29] At low T, we assume that the molecules are always in the $J=0$ rotational state. At higher T, contributions from the $J=1$ state will also yield anisotropic interactions. The energy difference between these two states is known to be 100 and 170 K for D_2 and H_2, respectively.[29] Thus for $T<50$ K, it is a good approximation to assume that all the molecules are in the spherical ($J=0$) state. Estimation of U_{10} are more complicated. A self-consistent phonon calculation for the commensurate $\sqrt{3}\times\sqrt{3}$ phase by Novaco[37] gives $U_{10}/k_B=-7.7$ and -8.1 K for H_2 and D_2, respectively. The difference is associated with the mass difference between the two molecules which gives a higher zero-point motion for H_2 than for D_2.

Using the data quoted above, we find $(\sigma^*,U^*)\simeq(1.2,0.22)$ for D_2 and (1.2,0.20) for H_2. However, for adsorbates we must also consider the following renormalization effects: (i) zero-point motion reduces the particle-particle interactions. This is not taken into account in the above estimations of ϵ and σ, since they are obtained from high-temperature data; (ii) the 2D particle-particle interaction is smaller than that estimated from the 3D system for the same reason as in (i). These two effects reduce ϵ and increase σ leading to values of U^* and σ^* somewhat larger than estimates in the literature for 3D.

In our simulations we have used (1.3,0.333) and (1.3,0.167) for D_2 and H_2, respectively. Some simulations with other values of U^* have also been done. Figure 6 shows the studied points in the (σ^*,U^*) parameter space, together with the literature data for different systems. Our selected values give good qualitative agreement with the experimental phase diagrams of both systems. However, a quantitative comparison with experiments is difficult for two reasons: (i) an accurate relation is un-

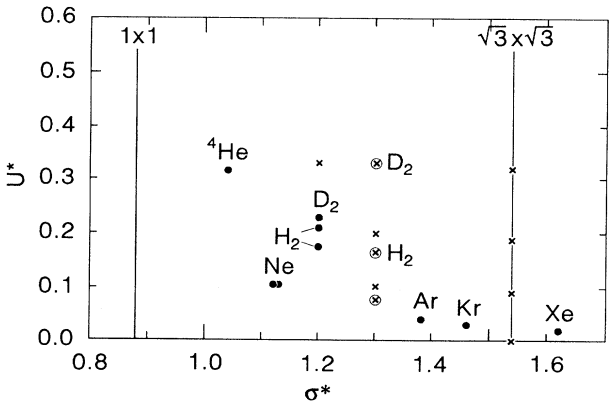

FIG. 6. Parameter space of our model. × indicates MC simulation points, and ⊗ indicates the best fit with H_2 and D_2. Values for other systems are collected from the literature: data for Ne, Ar, Kr, and Xe from Ref. 6, alternative values for Ne from Refs. 6 and 36, ^{4}He from Refs. 36 and 40, H_2 and D_2 from Refs. 29 and 37 and alternative values for H_2 from Refs. 29 and 41.

known between the experimentally reported coverage and that defined theoretically—substantial differences appear if one compares different experimental measurements;[12,17,18] (ii) the correct temperature scale depends on an absolute estimation of ϵ, which is not accurately known. A comparison between the melting temperatures at $\rho=1$ between the experiments[12] and our MC simulation gives $\epsilon/k_B=25$ K. This value is in agreement with the conclusion that the 2D value of ϵ should be smaller than the value estimated from the 3D system [$\epsilon/k_B=36.2$ (Ref. 29)], as discussed above. Experimentally, the coverage ρ is determined by assuming that $\rho=1$ for the coverage with the highest melting temperature.[12] This might be different from our definition $\rho=3N/N_s$, if the system exhibits nonhomogeneous density. In fact, in our simulations for low values of U^*, we have found a tendency for the formation of holes (low-density regions), even at $\rho=1$.

C. Results and discussion

Figure 7 compares experimental[12] (bottom) and simulated (top) phase diagrams for D_2 on graphite. The MC data have been obtained from the energy averages, as well as from the detailed study of the structure factor intensity of the different phases. Qualitative agreement between the different phase regions can be seen. However, the ϵ phase at the boundary between the γ and incommensurate phases is not found in the simulations. The transition lines between the fluid and gas phases are difficult to reproduce by the simulation (experimentally, they correspond to very broad peaks in the specific heat[12]). A detailed description of the phase diagram has not been attempted for H_2 on graphite. The same features appear except that there is no intermediate γ phase between the commensurate and incommensurate phases, in agreement with the experimental results.[13] Below, we concentrate on the case of D_2.

The simulations allow a detailed study of several quantities which are not observable, or only indirectly, in experiments. Figure 8 shows the energies versus temperature for different coverages. We obtained these results by increasing the temperature of our system from a long-time equilibrated low-temperature phase. (The method used to obtain good equilibrated phases is explained in Sec. III A.) We observe small features, kinks, and changes in slopes, at the transition points in the phase diagram of Fig. 7(a). We have not attempted to investigate the nature of all the transitions in detail. The melting transition for $\rho=1.336$ was investigated, however, and does show signs of hysteresis, characteristic of a discontinuous transition. The radially averaged structure factor $\bar{S}(q)$ is a very good indicator of the various structural phase transitions. It is shown in Fig. 9 for a number of coverages. It is obvious that peaks at different values of q grow and decay as a function of coverage. The intensity variation of the characteristic peaks in the nonaveraged $S(\mathbf{q})$ will be analyzed in detail below, but $\bar{S}(q)$ already shows the existence of several phases which we discuss below. In our simulations we have been able to scan a

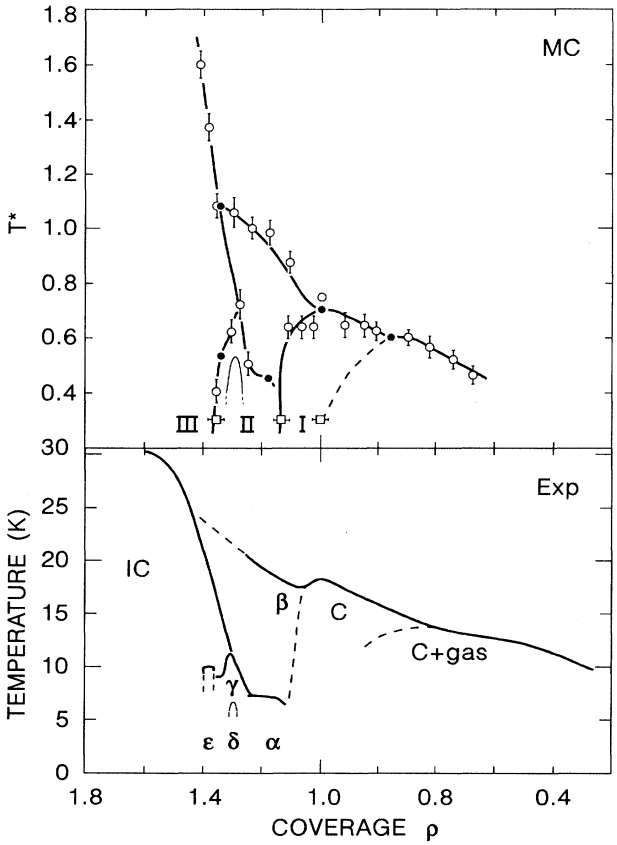

FIG. 7. Simulated (top panel) and experimental (Ref. 12) (bottom panel) phase diagrams for D_2 on graphite. The simulation data has been obtained from the E vs T scans for different coverages (indicated by ○ and ●) as well as from the analysis of the intensities of the different peaks in the structure factor with parameters $U^*=1/3$ and $\sigma^*=1.3$ (indicated by □).

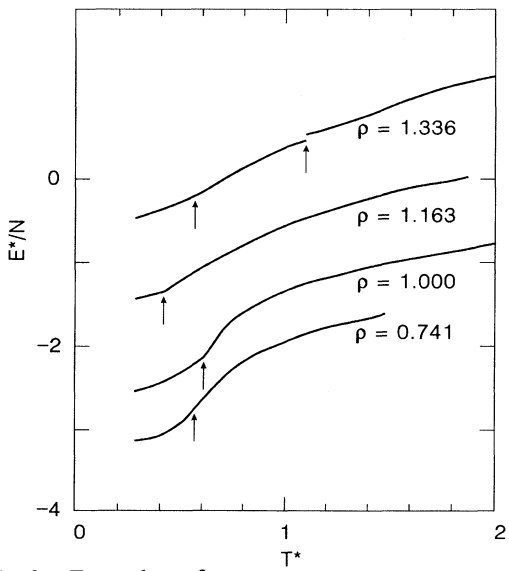

FIG. 8. Examples of energy vs temperature scans for different coverages obtained by MC simulations. Arrows indicate the positions of the different phase transitions.

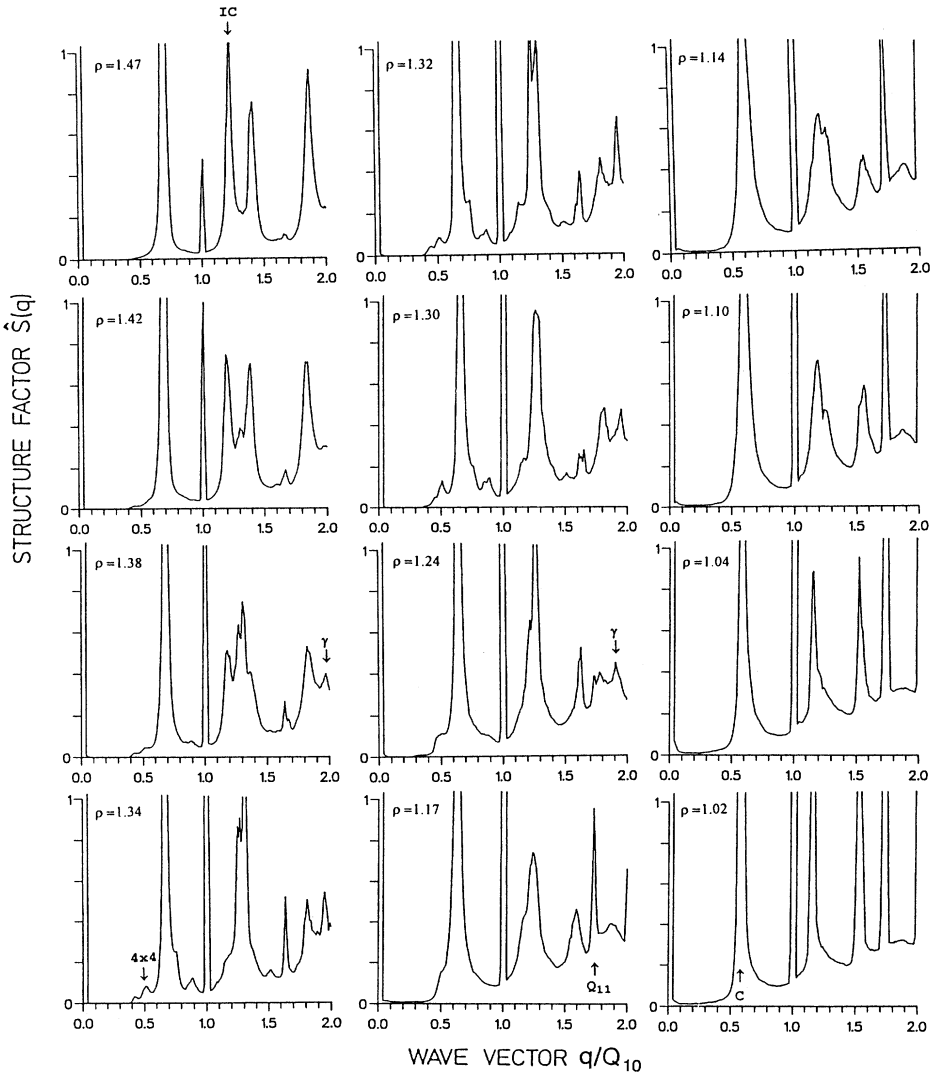

FIG. 9. Radial averages $\bar{S}(q)$ for different coverages at $T^*=0.3$. We have indicated some of the most interesting peaks characteristic of the different phases (incommensurate IC, γ, satellites of the 4×4 phase, and commensurate C), together with the Q_{10} and Q_{11} peaks. Many more features are evident in these plots.

much larger region in reciprocal space than is experimentally feasible so far. We begin by describing regions of the phase diagram with simple hexagonal phases.

1. *Commensurate phase*

At low coverages $0.8<\rho<1,1$, we find a commensurate, hexagonal phase. For smaller coverages this phase is stable, such that holes are formed in order to preserve the density of the $\sqrt{3}\times\sqrt{3}$ structured domains of registry A, B, and C. Domain walls with a local, relaxed structure reminiscent of that of the higher-density γ phase separate these domains. If the atoms are only marked in the A, B, and C positions (we call this the centered representation), the walls can generally be characterized as the conventional heavy and super-heavy walls. The tendency to form holes is enhanced for lower values of U^*.

2. *Fully incommensurate phase*

For high coverages, $1.4<\rho$, a dense hexagonal phase is stable. It is a twin structure, which is epitaxially rotated by angles $\pm\phi$. The twin or grain boundaries between the phases are low-density regions which contain precipitated defects—vacancies. This is illustrated in Fig. 10, which shows a snapshot of the simulation for 3969 particles ($\rho=1.47$) at $T^*=0.3$. We clearly see that there are predominantly two types of twin domains ($\pm\phi$). Furthermore, a few embedded defects and dislocation lines deform the structures, leading to difficulties in defining the epitaxial angles. In the relatively small grains it is difficult to determine if the dislocations prefer to form pairs (not destroying the long-range orientational order) or if they are isolated. Experimentally, it is possible that the grains might be larger due to the longer available time for reaching the equilibrium state. However, the simulated size corresponds closely to the single crystallites of Papyex samples of graphite.[18] On the XYZ graphite, the crystallites may be up to ten times larger. The simulations are, therefore, made on rather realistic size samples. The problem of the metastable—or not fully relaxed states—may be a real experimental feature, albeit exaggerated in the simulations. Their main effect is enhanced regions of coexisting phases as a function of coverage.

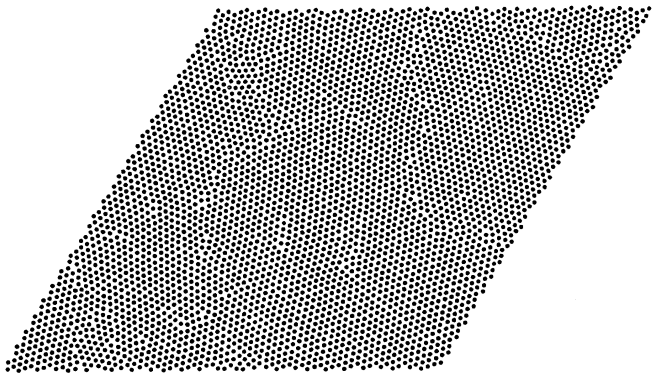

FIG. 10. Real-space snapshot corresponding to the simulated incommensurate phase ($T^*=0.3, N=3969$). Two coexisting domains rotated by $\pm\phi$ and separated by low-density domain walls can be seen.

3. *The γ phase*

For intermediate coverages, $1.1<\rho<1.4$, several interesting phases appear. We can understand these as phases in which the defects (vacancies) play an active role—namely, as elements of the structure. The vacancies are dissolved in the adsorbate, and the phase transition between the high- and intermediate-coverage phases can be thought of as a transition between a phase separated and a solvable state for the vacancies. The structures are strongly relaxed around the vacancies. Figure 11(a) shows the real-space snapshot of the γ phase with large relaxations screening the vacancies. On the right we show the same structure with the particles registered at the center of the cells (centered representation). This reveals the vacancies clearly, and demonstrates that dislocations tend to form a dense set of dislocation pairs. It is important to note that there is no perfect superlattice in the predominant part of the γ-phase region. The γ phase is stabilized by the diffuse scattering from the imperfect structure. As explained in Sec. II C, this phase can be understood as a strongly $2q$-modulated phase, or, in other words, a hexatic phase with irregular pairs of dislocations. The weak melting transition to a structured liquid corresponds to the loss of orientational order.

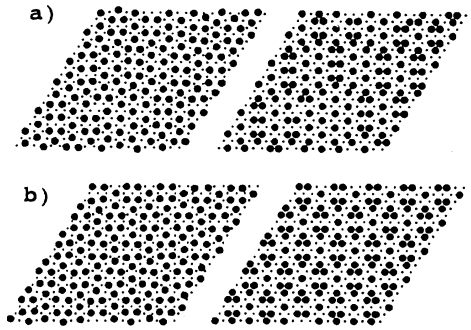

FIG. 11. Small sections of a real-space snapshot corresponding to (a) the γ phase and (b) the 4×4 superstructure. The pictures on the right are the same but with the particles centered in the nearest substrate wells (centered representation).

For a particular coverage $\sqrt{\rho}=\sqrt{21}/4$, the vacancies can be ordered in a perfect superlattice forming the 4×4 structure. This is shown in Fig. 11(b) (with the corresponding centered representation on the right). When relaxed, this superlattice gives rise to superlattice peaks at multiples of those of $\frac{1}{4}$ of the substrate unit cell. Comparison with available experimental data[17,18] gives good agreement for the peak positions and the relative intensities of the peaks. This proves that the real space picture of the 4×4 phase [Fig. 11(b)] obtained from our simulations is similar to that found experimentally for D_2. We emphasize that the simulations of $\bar{S}(q)$ for the large accessible region of the reciprocal space show characteristic features of this phase which have not yet been found experimentally. It would be extremely interesting to see this region investigated experimentally for D_2 (and other systems).

4. *The α phase*

From the specific heat[12] and the LEED (Ref. 17) experiments another phase at low coverages, $1.1<\rho<1.2$, has been suggested. Figure 12(a) shows the real-space structure for $\rho=1.104$ and Fig. 12(b) the corresponding centered representation of the same region. It is not a

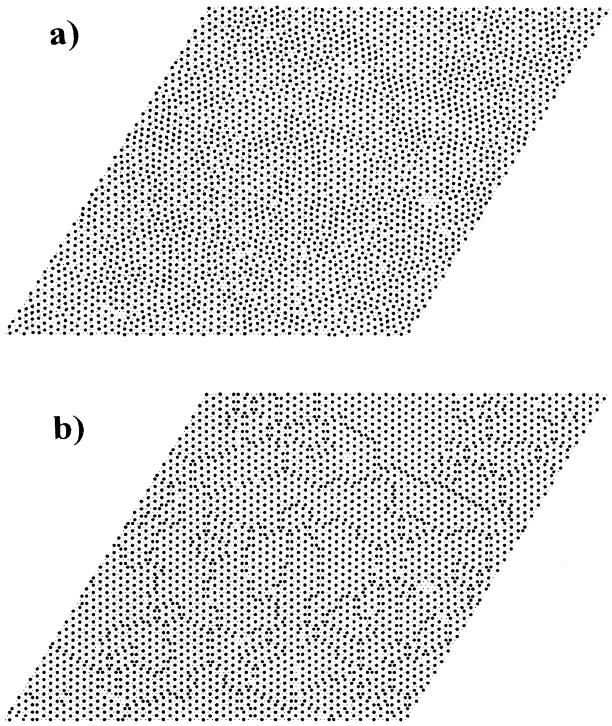

FIG. 12. (a) Real-space snapshot of the α phase for $T^*=0.3$ and $\rho=1.104$. (b) The same, but with the particles centered on the substrate wells (centered representation). A, B, and C registered domains can be seen, separated by meandering domain walls.

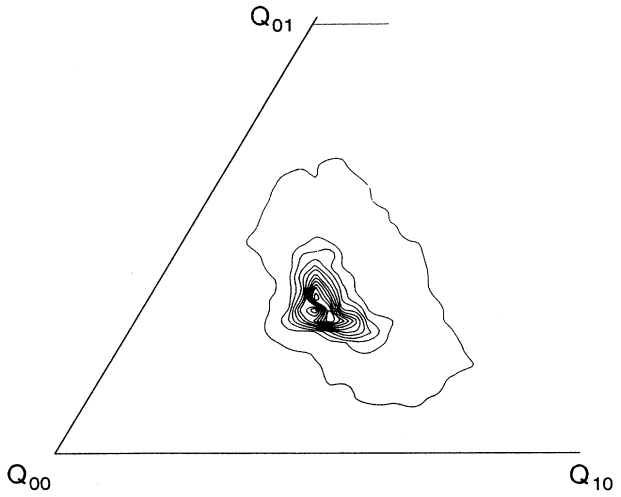

FIG. 13. Contour plot of $S(\mathbf{q})$ in the α phase showing the splitting of the $\mathbf{q}_{10}$ peak ($T^*=0.3$ and $\rho=1.104$). The behavior is similar to that found by LEED measurements in D_2 on graphite.

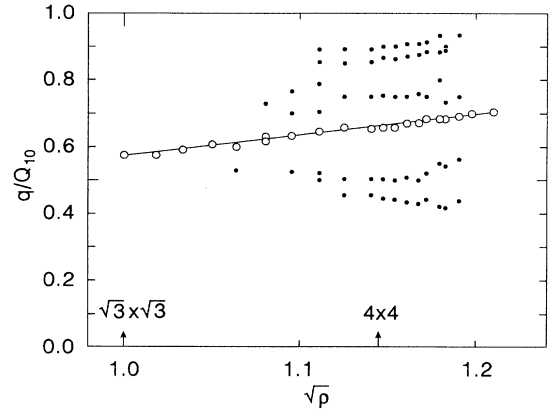

FIG. 14. Position of the main peak of the adsorbate $|\mathbf{q}_{10}|$ as a function of $\sqrt{\rho}$ for $T^*=0.3$. The positions of the satellites are also shown.

striped phase, as suggested on the basis of observed asymmetry in the LEED patterns. Rather, it is a meandering-domain-wall phase, where the domain walls of the γ phase separate regions of A-, B-, and C-registered $\sqrt{3}\times\sqrt{3}$ domains. It is possible that these domain walls give rise to the stripelike features in the scattering patterns. In order to test this idea, we have plotted in Fig. 13 an intensity contour plot of the scattering intensity around the $\mathbf{q}_{10}$ position. We find a behavior similar to that observed in the LEED experiments. We conclude that in our pure system (free from substrate surface steps and other imperfections) there is no evidence for a striped phase. In fact, we raise the question of whether the α phase is a proper phase at all, or whether it is an intermediate, meandering domain-wall "phase". For a further discussion of that phase we refer to Coppersmith *et al.*[38] and references in there.

5. *Coverage dependence of $S(\mathbf{q})$ and E*

In our simulations, we have been able to determine the structure factor over the first two substrate reciprocal-lattice cells (i.e., up to $\mathbf{Q}_{22}$). Two-dimensional contour plots of the intensity of $S(\mathbf{q})$ have been published elsewhere.[39] Here, we shall discuss a number of quantitative features by calculating the intensity of selected peaks, which are characteristic for the various phases discussed above.

The position of the dominant substrate peak $\mathbf{q}_{10}$ is shown in Fig. 14. It decreases linearly with $\sqrt{\rho}$, showing that the adsorbate lattice expands until hole formation becomes more favorable. It is this monotonic variation of $|\mathbf{q}_{10}|$ which makes possible the several phases observed both experimentally and in the simulations for intermediate coverages. In the γ-phase region, near the 4×4 value for $|\mathbf{q}_{10}|=Q_{10}\sqrt{7}/4$, superlattice satellites occur. The wave vectors for these satellites are also indicated in Fig. 14. Close agreement with experimental behavior[18] is found. We do not find evidence for even larger-unit-cell structures, as might be expected on the basis of the coincidence lattice models,[22] in which a whole devil's staircase of lock-in transitions should occur. The reason for this is either that the simulations are made for systems for which the size is too small and the equilibration time too short in order to enable such large-unit-cell structures to stabilize—or that it is a small-unit-cell imperfect structure, a hexatic phase, which is stabilized by the disorder diffuse scattering, as discussed in Sec. II C. Our data and the experiments support the latter picture.

In Fig. 15 we show the epitaxial angle ϕ in the various regions with variable coverage $\sqrt{\rho}$. Perfect agreement is

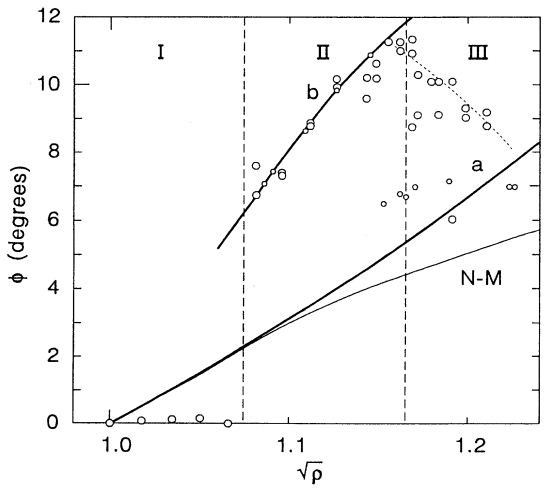

FIG. 15. Epitaxial rotation angle vs $\sqrt{\rho}$ for $T^*=0.3$. Experimental data corresponding to D_2 on graphite are also plotted. Lines correspond to (a) the theoretical relation and (b) the Novaco-McTague theory (Ref. 19) for $\eta=2$. The dotted line corresponds to the semicoincidence lattice model.

obtained with experiments in region I (nonrotated $\sqrt{3}\times\sqrt{3}$ structure) and region II (defect stabilized structure). The agreement is not as good in region III (elastically stabilized structure). Both experiments and simulations show good agreement with theory in region I (nonrotated) and II [relation (b) in Fig. 4], but again poorer agreement in region III [relation (a) in Fig. 4]. We expect that the difficulties in region III are due to the interplay between several effects: elastic, vacancy defects, and finite-size effects of the grains. This leads to poorly defined angles ϕ and also, as we have observed, to coexistence of several imperfectly rotated grains (as discussed in connection with Fig. 14). Nevertheless, a tendency for the simulation results to follow the relation predicted from the semicoincidence lattice theory (dotted line) is seen.

In Fig. 16 we have plotted the intensity variation of several of the characteristic peaks of $S(\mathbf{q})$. We notice a strong variation with coverage. The growth and decay of the intensities indicate that the different phases are in good agreement with the phase diagram (Fig. 7). We also notice large coexistence regions, presumably due to nonequilibrium features. We emphasize, however, each point is obtained independently from quenches from the high-temperature phases (as explained in Sec. III A).

The intensity of the $\mathbf{Q}_{10}$ peak in the structure factor is the most interesting one, since that gives the largest contribution to the energy integral in Eq. (5). It is the driving mechanism for gaining the energy from the corrugation potential as shown in Sec. II A. In Fig. 17 we show $S(\mathbf{Q}_{10})$, together with $S(\mathbf{Q}_{11})$, as a function of coverage and for $T^*=0.3$. It is clear that the increasing disorder at lower coverages allows the particles to occupy more favorable positions (near the center of the cells) and thus to gain energy until the corrugation potential locks the particles into the $\sqrt{3}\times\sqrt{3}$ structure at $\rho\simeq 1$. We notice a small increase in $S(\mathbf{Q}_{10})$ above the smooth, monotonic increase, in the region where there is a lock-in to the 4×4 structure. The extra increase is not observed in $S(\mathbf{Q}_{11})$. This demonstrates that the structure-formation process is

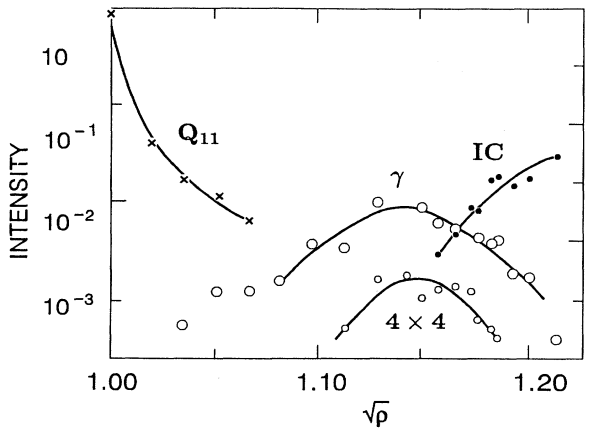

FIG. 16. Intensity of the most characteristic peaks of the structure factor $S(\mathbf{q})$ as a function of $\sqrt{\rho}$ for $T^*=0.3$. The identifications and relative positions of these peaks are shown by the radial averages $\bar{S}(q)$ in Fig. 9.

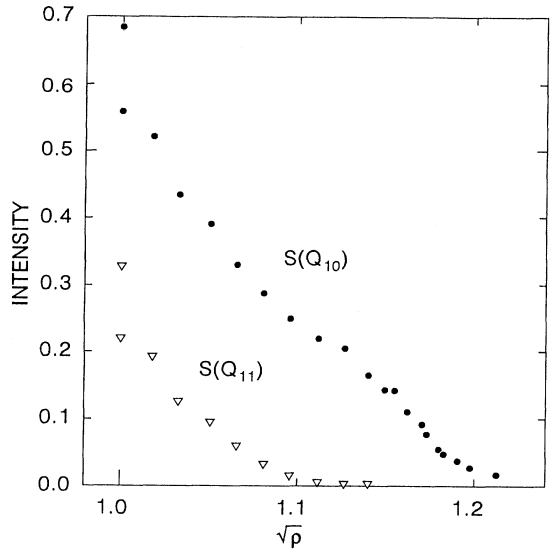

FIG. 17. Intensity of the $S(\mathbf{Q}_{10})$ and $S(\mathbf{Q}_{11})$ peraks as a function of $\sqrt{\rho}$ for $T^*=0.3$.

strongly nonlinear (as discussed by Reiter and Moss[8]) and that further relaxation and modulation of a rotated phase may lead to further energy gain. This may be enough to destroy the stability of nearby rotated phases, which are optimal from a linear point of view, but for which $\mathbf{q}_{10}$ does not correspond to the correct 4×4 structure. This lock-in effect is clearly seen in Fig. 14.

Finally, a few remarks about the effect of the magnitude of the corrugation potential. In Fig. 18 we show the

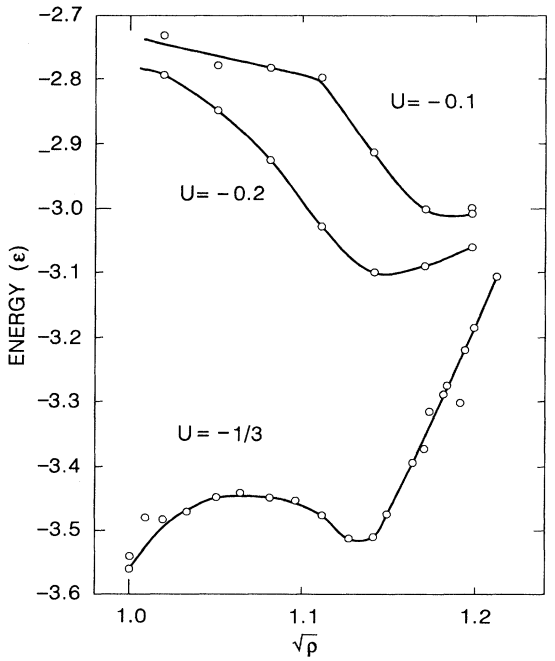

FIG. 18. Energy vs $\sqrt{\rho}$ for $T^*=0.3$ and different values of U^*.

energy for $T^*=0.3$ for different values of U^*. The case $U^*=\frac{1}{3}$ discussed above has been most intensively studied. For decreasing U^* the lock-in phases for intermediate coverages disappear and the lattice expands at the expense of the energy—presumably in order to gain entropy. For small U^* and at low coverages we notice the energy becomes independent of coverage. This is due to hole formation, indicating that for $\sigma=1.3$ the particles prefer to form connected regions by forming holes to preserve the optimum density. This suggests a new class of transitions in which the formation of holes or islands is an important element of the phase stabilization. The holes and islands are of course easily seen in the real-space pictures of the simulations. In $\bar{S}(q)$, the dominant effect is the appearance of diffuse small-angle scattering around $q=0$. This can be seen in Fig. 9 for the case $\rho\rightarrow 1$.

IV. SUMMARY AND CONCLUSIONS

We have studied adsorbed particles on a corrugated substrate, with special attention to the case of H_2, D_2, and the rare gases on graphite. These are examples of 2D systems that exhibit competition between the particle-particle and particle-substrate interactions.

Firstly, we presented a general theoretical model (Sec. II). For systems close to the $\sqrt{3}\times\sqrt{3}$ structure, and when the first term U_{10} of the Fourier transformation of the substrate potential is dominant, we have shown that the particle-substrate energy is determined by the Fourier transform of the density $\hat{\rho}(\mathbf{q})$ at $\mathbf{q}=\mathbf{Q}_{10}$. We have used our theory to study the epitaxial rotation angles ϕ as a function of the misfit m between the adsorbate and the substrate structures. For perfect, infinite incommensurate adsorbates no preferred value of ϕ is selected. Existing theories[19] consider only elastic deformations of the adsorbate to determine the dependence of $\phi(m)$ on the misfit m. We further propose that deformations around vacancies lead to another relation which explains a large number of available experimental data. We have also analyzed the role played by the finite size of the adsorbed islands or grains, and we have shown that this can give other $\phi(m)$ relations.

Secondly (Sec. III), we have performed MC simulations for the case of D_2 on graphite. The obtained phase diagram (as a function of T and ρ) is in good agreement with that measured by calorimetry.[12] The structure factors obtained from our MC data is also in agreement with LEED (Ref. 17) and neutron-scattering data.[18] In contrast to experiments, the possibility of calculating $S(\mathbf{q})$ for large values of q gives new information about the structure of the intermediate phases appearing between the commensurate and the incommensurate regions. In particular, from our simulations, we have determined the structures of the γ phase to be hexatic and found the real-space structure of the further modulated 4×4 phase. No evidence for stripes in the α phase was found. The epitaxial rotation angle exhibited by the different phases in our simulations is in agreement with experiments[17] and with the developed theory.

ACKNOWLEDGMENTS

We thank S. Fain and A. Sandy for a critical reading of the manuscript. We acknowledge J. Bohr, F. Grey, and P. Harris for fruitful comments. E. V. also acknowledges the hospitality of the Physics Department of the Risø National Laboratory and the Ministerio de Educación y Ciencia (Spain) for financial support.

*On leave from Department E.C.M., Universitat de Barcelona, Diagonal 647, 08028 Barcelona, Catalonia, Spain.

[1]A. G. Naumovets, Contemp. Phys. **30**, 187 (1989).
[2]K. J. Strandburg, Rev. Mod. Phys. **60**, 161 (1988).
[3]J. D. Brock *et al.*, Z. Phys. B **74**, 197 (1989).
[4]P. W. Anderson, Mater. Res. Bull. **8**, 153 (1973); P.-A. Lindgård, Phys. Rev. Lett. **61**, 629 (1988); C. L. Henley, *ibid.* **62**, 2056 (1989).
[5]J. A. Krumhansl, Phys. Today **44** (3), 34 (1991); P.-A. Lindgård and O. G. Mouritsen, Phys. Rev. Lett. **57**, 2458 (1986); Phys. Rev. B **41**, 688 (1990).
[6]J. Villain and M. B. Gordon, Surf. Sci. **125**, 1 (1983).
[7]M. S. Dresselhaus and G. Dresselhaus, Adv. Phys. **30**, 139 (1981).
[8]G. Reiter and S. C. Moss, Phys. Rev. B **33**, 7209 (1986).
[9]C. Girardet and C. Girard, Phys. Rev. B **39**, 8643 (1989).
[10]R. Marx, Phys. Rep. **125**, 2 (1985).
[11]D. S. Greywall and P. A. Busch, Phys. Rev. Lett. **67**, 3535 (1991).
[12]H. Freimuth and H. Wiechert, Surf. Sci. **178**, 716 (1986).
[13]H. Freimuth, H. Wiechert, and J. Lauter, Surf. Sci. **189**, 548 (1987).
[14]Hawoong Hong *et al.*, Phys. Rev. B **40**, 4797 (1989).
[15]P. S. Schabes-Retchkiman and J. A. Venables, Surf. Sci. **105**, 536 (1981).
[16]S. Calisti, J. Suzane, and J. A. Venables, Surf. Sci. **115**, 455 (1982).
[17]J. Cui and S. C. Fain, Phys. Rev. B **39**, 8628 (1989).
[18]H. Freimuth, H. Wiechert, H. P. Schildberg, and H. J. Lauter, Phys. Rev. B **42**, 587 (1990).
[19]A. D. Novaco and J. P. McTague, Phys. Rev. Lett. **38**, 1286 (1977); J. Villain, *ibid.* **41**, 36 (1978); J. P. McTague and A. D. Novaco, Phys. Rev. B **19**, 5299 (1979); H. Shiba, J. Phys. Soc. Jpn. **46**, 1852 (1979); **48**, 211 (1980).
[20]P. Bak, D. Mukamel, J. Villain, and K. Wentowska, Phys. Rev. B **19**, 1610 (1979).
[21]D. L. Doering and S. Semancik, Surf. Sci. Lett. **175**, L730 (1986); Phys. Rev. Lett. **53**, 66 (1984).
[22]C. R. Fuselier, J. C. Raich, and N. S. Gillis, Surf. Sci. **92**, 667 (1980).
[23]S. Aubry, in *Solitons and Condensed Matter Physics*, edited by A. R. Bishop and T. Schneider (Springer, Berlin, 1978), p.

264.
[24]A. D. Novaco, Phys. Rev. B **22**, 1645 (1980).
[25]P. Zeppenfeld, J. Becher, K. Kr. David, R. L. Palmer, and G. Comse, Phys. Rev. B **45**, 5179 (1992).
[26]J. Cui, S. C. Fain, H. Freimuth, H. Wiechert, H. P. Schildberg, and H. J. Lauter, Phys. Rev. Lett. **60**, 1848 (1988).
[27]S. C. Moss, G. Reiter, J. L. Robertson, C. Thompson, J. D. Fan, and K. Ohshima, Phys. Rev. Lett. **57**, 3191 (1986).
[28]N. D. Mermin, Phys. Rev. **176**, 250 (1968).
[29]I. F. Silvera, Rev. Mod. Phys. **52**, 393 (1980).
[30]E. Vives and P.-A. Lindgård, Phys. Rev. B **44**, 1318 (1991).
[31]M. A. Krivoglaz, *Theory of X-Ray and Thermal-Neutron Scattering by Real Crystals* (Plenum, New York, 1969).
[32]F. Grey and J. Bohr, *Phase Transitions on Surface Films, NATO Advanced Studies Institute Series B: Physics,* edited by H. Taub (Plenum, New York, 1990); Europhys. Lett. **18**, 717 (1992); J. Bohr and F. Grey, Condensed Matter News **1**, 12 (1992). (We remark that data for D_2 on graphite, which in their picture comparing theory and experiments is plotted for $m > 1$, should have been plotted for $m < 1$.)
[33]K. L. D'Amico, J. Bohr, D. E. Moncton, and Doon Gibbs, Phys. Rev. B **41**, 4368 (1990).
[34]S. M. Paik and I. K. Schuller, Phys. Rev. Lett. **64**, 1923 (1990).
[35]K. Kern, P. Zeppenfeld, R. David, R. L. Palmer, and G. Comse, Phys. Rev. Lett. **576**, 3187 (1986).
[36]G. B. Huff and G. J. Dash, J. Low-Temp. Phys. **241**, 155 (1976), and references therein; more recent estimations can be found in X. Z. Ni and L. W. Bruch, Phys. Rev. B **33**, 4584 (1986), and references therein.
[37]A. D. Novaco, Phys. Rev. Lett. **60**, 2058 (1988).
[38]S. N. Coppersmith, D. S. Fisher, B. I. Halperin, P. A. Lee, and W. F. Brinkman, Phys. Rev. B **25**, 349 (1982).
[39]E. Vives and P.-A. Lindgård, Surf. Sci. Lett. (to be published).
[40]M. W. Cole, D. R. Frankl, and D. L. Goodstein, Rev. Mod. Phys. **53**, 199 (1981).
[41]Z. C. Guo and L. W. Bruch, J. Chem. Phys. **77**, 1417 (1982).